J Nanostruct 10(4): 871-879, Autumn 2020

RESEARCH PAPER

Laser Ablation based "Green" Synthesis of multilayer Graphene and Graphene Oxide nanosheets

Elnaz Vaghri

Young Researchers and Elite Club, Shahr-e-Qods Branch, Islamic Azad University, Tehran, Iran

ARTICLE INFO

Article History:
Received 27 July 2020
Accepted 16 September 2020
Published 01 December 2020

Keywords:
Carbon nanostructures
Cetyltrimethylammonium bromide
Graphene
Graphene Oxide
Liquid nitrogen
Pulsed laser ablation

ABSTRACT

In this experimental investigation, a simple and efficient technique is presented for the carbonic nanostructures fabrication-in particular, Graphene Oxide (GO) and Graphene nanosheets- based on the pulsed laser ablation of graphite target inside the Cetyltrimethylammonium bromide (CTAB) (0.1 M) and liquid nitrogen environments using the pulsed nanosecond Q-switched Nd:$Y_3A_{l5}O_{12}$ (Nd:YAG) laser at 532 nm. X-ray diffraction (XRD) pattern, Raman spectrum, Transmission electron microscopy (TEM), Fourier transform infrared spectroscopy (FT-IR) and Field emission scanning electron microscopy (FE-SEM) were used to characterize the ablation products. Results represent the formation of multilayer graphene and GO nanosheets in liquid nitrogen medium and CTAB solution, respectively. In liquid nitrogen medium, the graphene nanosheets includes the largest SP^2 domain size and the least defects, while the size distribution of SP2 domains of GO nanosheets decreased noticeably in CTAB solution that can be related to the breaking of crystallites with oxidation. The XRD spectra of the produced samples showed the well-defned crystalline structure of the hexagonal phase of CNx in liquid nitrogen medium and also the formation of GO and other new carbonic structures in CTAB solution. In addition, the stretching vibrations of C=O and C-O in carboxylic groups of GO structure and vibrations of graphitic domains (C=C bonds) in graphene nanosheets was observed by FTIR spectra. Our experimental results can be useful guidance toward the production of graphene nanosheets with desired attributes.

How to cite this article
Vaghri E. Laser Ablation based "Green" Synthesis of multilayer Graphene and Graphene Oxide nanosheets. J Nanostruct, 2020; 10(4): 871-879. DOI: 10.22052/JNS.2020.04.020

INTRODUCTION

During the last years, graphene, a one-atom-thick hexagonal array of SP^2-bonded carbon atoms packed into a two-dimensional honeycomb structure, has aroused intensive research interest from both industry and the research community. [1]. Graphene offers a wide range of exceptional properties [2-5], that make this 2-dimensional carbon allotrope scientifically very fascinating and commercially essential for numerous industrial applications such as hydrogen storage [6], drug delivery [7], electric devices [8], supercapacitors [9], solar cells [10] and memory cells [11]. In addition, graphene is demonstrated to be suitable candidates for fabricating a gas sensing device owing to its intrinsic properties such as large surface area, higher interaction with gas molecules, and zero rest mass of its charged carriers [12]. Furthermore, graphene oxide (GO), which is the functionalized form of graphene, contains epoxy (-O-), hydroxyl (-OH), carbonyl (-C=O) and carboxyl (-COOH) groups [13, 14], has been considered as strategic

* *Corresponding Author Email: elnaz.vaghri@gmail.com*

nanomaterials for a lot of applications including; electronics, biosensors, pipes, semiconductors, and packaging because of its extraordinary electrochemical properties. Despite the fact that graphene demonstrate far exceptional properties, the high hydrophobic character of graphene makes it easy to form irreversible aggregation or even restack owing to strong π-π stacking interaction and Van der Waals forces [15]. Studies indicate that introducing protective reagents and surfactants to the graphene surface, such as octadecylamine [16], silicone [17], polystyrene [18], hexadecyltrimethylammonium bromide (CTAB) [19] and dodecyltrimethylammonium bromide (DTAB) could partially improve this problem [20]. CTAB is a type of cationic surfactant which is consists of a cationic polar head and a hydrophobic tail which enables it either to agglomerate negatively charged nanoparticles and to use the hydrophobic effect [21, 22]. In fact, when the CTAB insertion in the interlayer of GO nanosheets, the positively charged groups of the CTAB allows it to easily assemble with the negatively charged carboxyl group of GO and interact electrostatically with the π cloud of GO [22, 23], this phenomenon can effectively resolved the aggregation problem of GO nanosheets. The initial goal of the scientist was finding new routes for the easy and proficient preparation of graphene-based materials. In the last few years, several methods include chemical or physical methods have been devised to fabricate graphene nanosheets such as pulse laser ablation (PLA), chemical vapor deposition (CVD), epitaxial growth, micromechanical exfoliation, chemical oxidation-reduction of graphite and some other specific techniques. Using chemical techniques we may have lots of amount of graphene or graphene oxide in one experiment by there is not any effective tool to control the quality of sheets i.e. area of sheets or number of layers [24]. Furthermore, most of the chemical techniques require organic solvents while production process which may cause toxic deposits [25], which are highly unpleasant in view of industrial and medical applications and for green chemistry. Using physical techniques, such as Laser ablation method, the rate of production is lower but these methods include friendly environmental process [24]. In addition, the purity of the products is higher than in comparison with chemical methods. Among them, pulsed laser ablation in liquids (PLAL) has illustrated to be an impressive and useful technique to produce high-quality nanoparticles (NPs) of a wide range of materials [25]. PLAL technique containing different benefits in comparison with traditional methods previously cites such as green chemistry process, controllable and uniform nano material size with less than 100 nm, cleaner and faster process, ability to construct complex structure compounds, ability to modify the surface of nanoparticles, etc [25]. Although several studies have been reported on the effects of laser parameters on the characteristics of carbon nanostructures [26-30], there is a lack of experimental study about the effect of liquid medium environment on the characteristics of graphene nanosheets. In the present study, carbon nanostructures in particular, graphene and GO nanosheets are produced using the second harmonics of an Nd:YAG laser in liquid nitrogen and CTAB solution environments and then the effect of liquid environment on the characteristics of final products have been investigated experimentally. The rapid cooling of the irradiated target surface, which can minimize the destructive laser processing side reactions, is the outstanding property of liquid nitrogen medium [29, 31]. In addition, the liquid nitrogen molecules can be easily penetrated into spaces between graphite layers during laser heating and the cryogenic liquid evaporates during laser ablation. The gaseous phase developed and leads to separation sheets of graphene from the layered structure of graphite [26, 29]. These are the important point of employing liquid nitrogen as another ablation environment in this experiment.

MATERIALS AND METHODS

In the present investigation, graphene nanosheets and carbon nanostructures solutions were fabricated by the pulsed laser ablation of a graphite plate (%99 purity) in liquid nitrogen (-195.79°C) and cetyltrimethylammonium bromide (CTAB) 0.1 M solution environments using a Q-switched Nd:YAG laser at 532 nm. At first the graphite target was placed on the bottom of an open cylindrical glass vessel flled with 20 mL of liquid. Height of liquid on the surface of the target was 0.8 cm. Before starting the experiment, the graphite target and containers were cleaned ultrasonically in alcohol, acetone and deionized water solutions respectively for 15 min to remove any residual contaminants. The graphite plate was ablated with the second harmonic of a Nd:YAG laser operated at 7-ns pulse width and 5-Hz repetition rate. Output beam of laser was 6 mm, which was

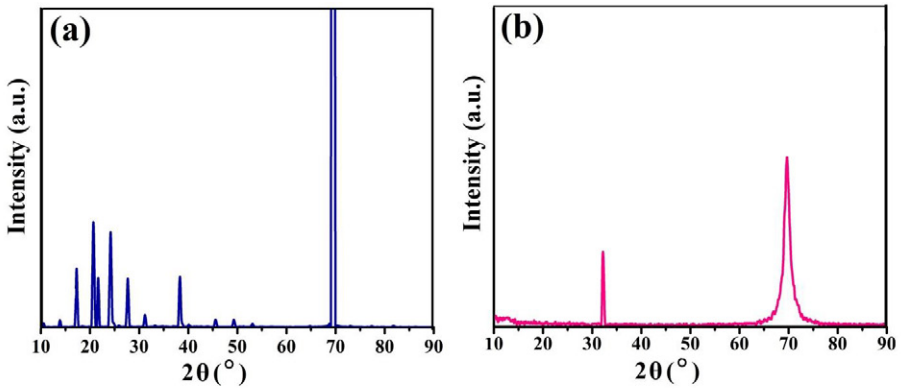

Fig. 1. X-ray diffraction of carbon nanostructures produced in (a) CTAB solution and (b) liquid nitrogen medium

focused by a 58-nm focal length lens on the surface of the target. The fluence of the laser pulse for producing graphene nanosheets was 0.5 J/cm^2. To achieve a thermal steady state condition during the ablation process, liquid nitrogen is added into glass cylindrical vessel continually. After laser exposure, owing to the evaporation of liquid nitrogen at the room temperature, the cylindrical vessel was filled with de-ionized (DI) water gradually. A variety of analytical techniques have been used to study and characterization of synthesized products. Infra-red transmission spectra of the produced samples are characterized using a NEXUS 870 FT-IR spectrometer from thermo Nicolet Co. The crystalline structure of the dried carbon nanostructures suspensions on silicon substrates are evaluated by X-ray diffraction (XRD) with Cu-Kα radiation (λ = 1.54060 Å), using a STOE–XRD diffractometer. The surface morphology of the produced samples was investigated by Hitachi, S-4160 field emission scanning electron microscopy (FE-SEM). Raman Thermo Nicolet disperse spectroscope from Almega (light source: 532 nm Nd:YLF laser) is used to evaluated of structure and quality of produced graphene nanosheets in dried drops of suspensions on glass substrates with 0.1 cm^{-1} spectral resolution. Moreover, Transmission electron microscopy (TEM, Zeiss EM10C) micrographs are obtained by depositing a drop of the concentrated suspensions on carbon-coated copper grids.

RESULTS AND DISCUSSION

Crystallinity analysis

The X-ray diffraction patterns of produced samples in different liquid environments are shown in Fig. 1. In order to record XRD data, few drops of every suspension were dried on silicon substrates at room temperature.

X-ray diffraction pattern of the synthesized products in liquid CTAB solution indicates a weak peak at 2θ=10.41° attributes to the (002) reflection planes of GO structure [32]. Furthermore, another weak diffraction peak at 2θ=13.88° can be belongs to X-ray photons diffracted from CTAB (400) molecule. In addition, due to drying process of GO and deoxygenating of weak oxygen functional groups and restacking of graphene layers, diffraction peaks at 2θ=17.26° and 24.24° appeared in this pattern [33, 34]. As a significant difference with previous work [35], with increasing the concentration of CTAB from 0.04 to 0.1 M, we observed the new strong diffraction peak at 2θ=21.66°. Diffraction peak emerging at 2θ=20.68° is characteristic of fullerite (113) structure, while two other diffraction peaks at 2θ=21.66° and 2θ=31.19° indicate the Buckminsterfullerene structure in the suspension, corresponding to the (222) and (422) orientations, respectively. Moreover, the feature around 2θ=27.7° is corresponded to (002) reflection usually observed for graphitic materials [36]. Several diffraction peaks at 2θ=45.54°, 49.26° and 53.05° are detected that are attributed to (220), (022) and (311) reflection planes of carbon oxide structure, respectively. X-ray diffraction pattern of produced sample in liquid nitrogen medium, (Fig. 1b), shows a peak at 2θ=32.12° belongs to (200) reflection plane of hexagonal phase of carbon nitride (CNx) structure. Also, the peak of X-ray photons diffracted from (400) planes of Si substrate can be seen at 2θ=69.84° in these patterns. Increasing the intensity of X-ray diffraction peaks of produced carbonic materials in CTAB solution confirms a better crystallinity of the samples in this environment.

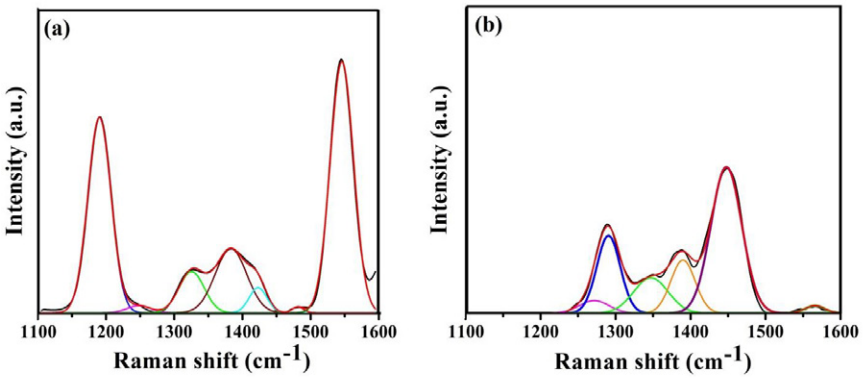

Fig. 2. Raman spectra of synthesized products (a) liquid nitrogen medium and (b) CTAB solution

Raman studies

Raman spectroscopy is a standard, powerful and non-destructive technique for studying and characterizing of carbon-containing materials such as diamond, graphene, diamond-like carbons, graphite and carbon nanotubes (CNT). The most noticeable features in Raman spectrum of graphene and graphite are the D, G and 2D (historically referred to as G') bands. The G band is the only Raman mode in graphene arising from a conventional first order Raman scattering process and attributes to the in-plane, zone center, doubly degenerate phonon mode (transverse (TO) and longitudinal (LO) optical) with E_{2g} symmetry [37], while the D and 2D modes originate from a second-order double resonant process between nonequivalent K points in the Brillouin zone (BZ) of graphene, involving two zone-boundary phonons (TO-derived) for the 2D and one phonon and a defect for the D band [38, 39]. Raman spectra of the produced samples measured by 532 nm excitation wave length of Nd:YLF laser in the frequency range from of 1100-1600 cm^{-1} are illustrated in Fig. 2.

Output data have been recorded from dried drops of every suspension on glass substrates. As shown in Fig. 2a, the Raman spectrum of produced sample in liquid nitrogen medium exhibits main characteristic peak at 1545 cm^{-1} correspond to the G-band and asymmetric Raman intensity distribution in the range 1100-1460 cm^{-1}. Therefore, the individual peaks of Raman spectrum were deconvoluted using Gaussian peaks to give the structural information in detail. The most intense peak appears at 1190 cm^{-1} in this spectrum is originated from highly disordered and wrinkled (defective) morphology of the graphene nanosheets [40], while the characteristic peak observed at around 1248 cm^{-1} corresponds to covalent C-N single bonds [41]. This result is in a very good agreement with XRD pattern. Furthermore, the individual peaks located at ~1380 cm^{-1} and 1325 cm^{-1} are belonging to the D-band and frequency of diamond lattice, respectively. Owing to phonon confinement effect, a triple-degenerated Raman band at 1333 cm^{-1} of bulk diamond crystal shifts to 1325 cm^{-1} in the 2-5-nm nanodiamond [42]. In addition, the other additional peak appears at ~1422 cm^{-1} and 1479 cm^{-1} in this spectrum are assigned to the vibration frequencies of Hg (7) mod from the C60 fullerene molecule and nanocrystalline diamond (NCD) [43, 44]. With changing the laser ablation environment to the CTAB solution, the Raman spectrum indicates change in the bands position and the shape (see Fig. 2b). The D-band for the GO nanosheets produced by 0.1 M concentration of CTAB is observed at the wave number of 1347cm^{-1}, while the G peak shift to higher wave number at 1565 cm^{-1} and becomes broadens. The change in the position of the G band is typically associated to a modification of the electronic structure of the carbon nanomaterial, being shifted to higher frequencies in the presence of electron-acceptor groups [35, 45]. In fact, the trimethylammonium moiety of CTAB molecule can act as an electron-acceptor group, thus causing a shift of the G band to higher wavenumber [45]. Moreover, the additional peaks at the wave numbers of 1290 cm^{-1} 1389 cm^{-1} can be seen in this spectrum which can belong to the carbon dioxide structure in the suspension [46]. The prominent peak appearing at 1447 cm^{-1} can be attributed to the nanodiamond [47]. Furthermore, another characteristic peak at 1271 cm^{-1}, is also clear, which is associated with SP^3

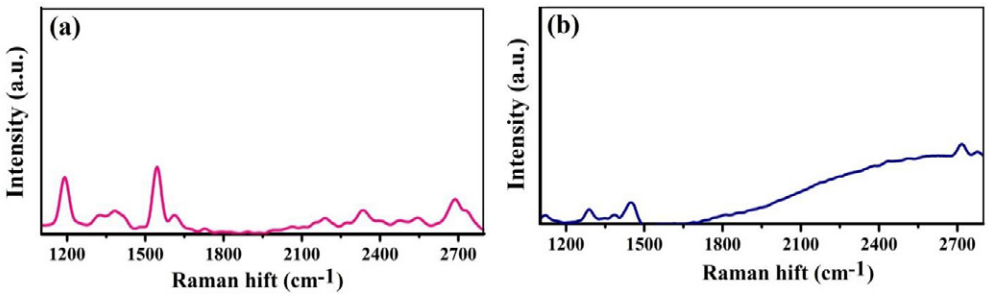

Fig. 3. Raman spectra of produced sample in the range of 1100-2800 cm^{-1} (a) liquid nitrogen and (b) CTAB solution

diamond bonding in tetrahedral amorphous carbon (ta-C) films [48]. The disorder-induced D band to that of the G band (I_D/I_G) has been widely used to acquire quantitative information about the amount of defects in the structure of carbonic materials and it is inversely proportional to the average crystallite size of SP^2 domains [49]. As can be seen in Raman spectrum of produced sample in liquid nitrogen medium (Fig. 2a), the prominent G band with intensity compared to the D band is suggestive of minor structural defects and disorders in graphene nanosheets which are produced in this cryogenic medium. In present investigation we observed that the intensity ratio, I_D/I_G, for the sample produced in CTAB solution was 4.67 and decreased to 0.26 in liquid nitrogen medium. In order to determine the average crystallite size of the SP^2 domains in graphene nanosheets, we employed the Tuinstra and Koenig relation, which relates the ratio of D and G bands intensities into the crystallite size as follows [27, 37]:

$I_D/I_G = [2.4 \times 10^{-10} (\lambda^4)] / L_a$ (nm)

where λ is the laser wavelength which was used for Raman spectroscopy, La is the average crystallite size of the SP^2 domains, I(D) is the intensity of the D band, and I(G) is the intensity of the G band. The calculated La values were found as 73.94 nm and 4.11 nm for produced sample in liquid nitrogen and CTAB medium, respectively. The results shows that the average crystallite size decreases with oxidation of graphene nanosheets in CTAB solution ; this may be owing the breaking of crystallites with oxidation resulting in the formation of defects, disorders, SP^3 hybridization and changes in crystallinity [50]. Furthermore, as shown in Fig. 3, at the far wave number side (2400-2800 cm^{-1}) another individual peaks at 2688 cm^{-1} and 2717 cm^{-1} (denoted as 2D bands) can be clearly seen. These bands are the characteristic peaks of the graphene structure and originates from double resonance Raman scattering. In monolayer graphene, the 2D Raman band occurs as a single peak near 2675 cm^{-1}, and this peak shifts to higher wavenumber side in case of multilayer graphene [51].

FT-IR characterization

For further investigating the changes in surface chemical compositions of produced sample in liquid nitrogen and CTAB solution the tests, FT-IR analysis was carried out in the range of 300-4000 cm^{-1}. It can be seen from Fig. 4(S_1), the FT-IR emission spectrum of produced sample in CTAB solution displays the strong band at 740 cm^{-1} attributed to C-H out-of-plane bending modes [52]. Furthermore, the absorption bands at 1640 cm^{-1} and 2358 cm^{-1} wavelength could be assigned to the stretching vibrations of C=O and C-O in carboxylic groups, respectively [53, 54].

In addition, we can observe the presence of hydroxyl groups (O-H stretching mode) of intercalated water molecule at 3413 cm^{-1} and some minor (low intensity) C-H stretching vibrations originate from the alkyl chain of CTAB molecule at 2927cm^{-1} and 2856cm^{-1} [55]. In the case of liquid nitrogen medium, the absorption peak at 732 cm^{-1} also is represent the out-of-plane bending of C-H modes, while the presence of absorption peak observed in the medium frequency area, at 1637 cm^{-1} is corresponded to the skeletal; vibrations of graphitic domains (C=C bonds) [55]. Moreover, the strong and broad absorption band at 3308 cm^{-1} is associated with -NH functional groups [56]. This broad absorption band also may be overlap with the O-H stretching vibration of water molecule in the range of 3200-3600 cm^{-1} Besides, the absorption bond in FT-IR spectra of all suspensions in the range of 2000-2200 cm^{-1} is belongs to

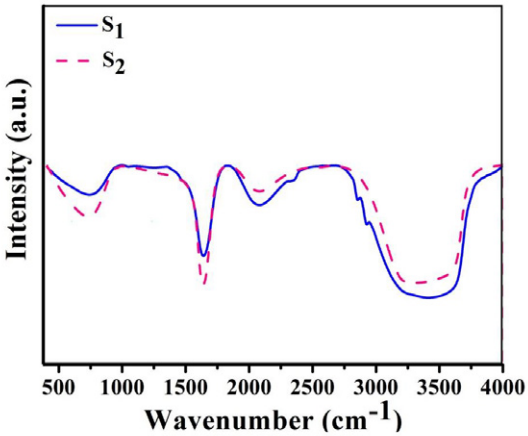

Fig. 4. FTIR spectra of produced samples in (s_1) CTAB solution and (S_2) liquid nitrogen environment

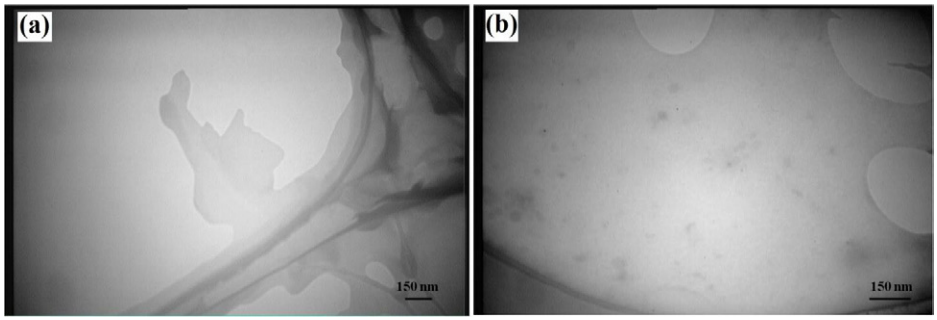

Fig. 5. TEM micrographs of the samples produced in; (a) CTAB solution and (b) liquid nitrogen medium

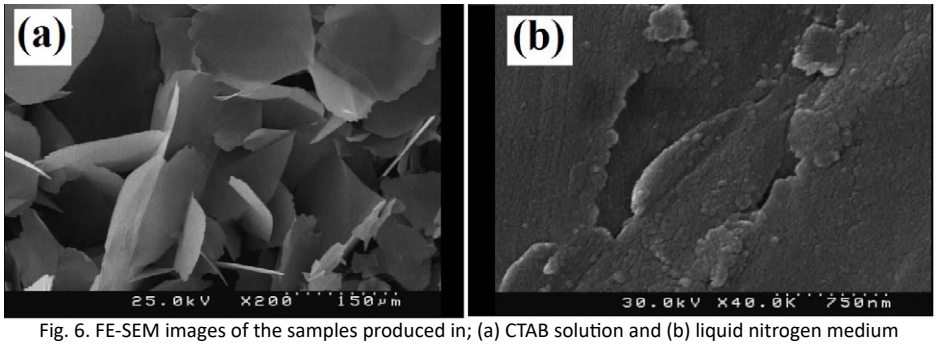

Fig. 6. FE-SEM images of the samples produced in; (a) CTAB solution and (b) liquid nitrogen medium

carbon-carbon triple bonds [57].

TEM and FE-SEM analysis

As shown in Fig. 5 the TEM micrographs of the surface of produced samples indicate the transparent silk-like morphology of graphene nanosheets.

More darkness in TEM image of produced sample in CTAB solution is attributed to the regions that several GO layers are stacked on each other. In addition, in liquid nitrogen medium, carbonic nanoparticles to form of dark points beside the graphene nanosheets can be clear observed. Fig. 6 illustrates the FE-SEM micrographs of the produced samples. The images show that all the products are composed of sheet-like structures in the suspensions, however, in CTAB solution; produced sheets are the GO nanosheets with well defined edges in the suspension.

Furthermore, it can be seen that in liquid

nitrogen medium the exfoliated-like structures was decorated with spherical structures. Results are in good agreement with TEM information.

CONCLUSIONS

In this study, carbonic nanostructures suspensions have been produced by focusing the second harmonic of Nd:YAG laser onto the graphite target in liquid nitrogen and CTAB (0.1 M) solution environments. According to the Raman spectra, the prominent G band with intensity comparable to the D band in spectrum of produced sample in liquid nitrogen medium is indicative of minor structural defects and disorders in graphene nanosheets which are produced in this medium. Furthermore, the size distribution of SP^2 domains of GO nanosheets decreased noticeably in CTAB solution that can be attributed to the breaking of crystallites with oxidation, resulting in the formation of disorders, defects and SP^3 hybridization. XRD data reveals that the crystallinity degree of samples is increased in CTAB solution. Also the XRD results indicate the formation of hexagonal phase of carbon nitrogen (CNx) structure in liquid nitrogen medium. Based on the TEM and FE-SEM image, graphene nanostructures are transparent sheet-like in the suspensions and size of transparent graphene nanosheets in order of hundreds nanometer. The FT-IR spectra represent the presence of stretching vibrations of C=O and C-O in carboxylic groups of GO structure and vibrations of graphitic domains (C=C bonds) in graphene nanosheets. Consequently, our experimental results indicate that the liquid nitrogen medium is the suitable medium for produce high-quality nanosheets whereas CTAB solution is the capable environments for producing GO nanosheets.

CONFLICT OF INTEREST

The authors declare that there is no conflict of interests regarding the publication of this manuscript.

REFERENCES

1. Li J, Miao D, Yang R, Qu L, Harrington PdB. Synthesis of poly(sodium 4-styrenesulfonate) functionalized graphene/cetyltrimethylammonium bromide (CTAB) nanocomposite and its application in electrochemical oxidation of 2,4-dichlorophenol. Electrochimica Acta. 2014;125:1-8.
2. Stoller MD, Park S, Zhu Y, An J, Ruoff RS. Graphene-Based Ultracapacitors. Nano Letters. 2008;8(10):3498-502.
3. Novoselov KS, Geim AK, Morozov SV, Jiang D, Katsnelson MI, Grigorieva IV, et al. Two-dimensional gas of massless Dirac fermions in graphene. Nature. 2005;438(7065):197-200.
4. Soldano C, Mahmood A, Dujardin E. Production, properties and potential of graphene. Carbon. 2010;48(8):2127-50.
5. Balandin AA. Thermal properties of graphene and nanostructured carbon materials. Nature Materials. 2011;10(8):569-81.
6. Wang K, Zhang X, Liu Y, Ren Z, Zhang X, Hu J, et al. Graphene-induced growth of N-doped niobium pentaoxide nanorods with high catalytic activity for hydrogen storage in MgH2. Chemical Engineering Journal. 2021;406:126831.
7. Mauri E, Salvati A, Cataldo A, Mozetic P, Basoli F, Abbruzzese F, et al. Graphene-laden hydrogels: A strategy for thermally triggered drug delivery. Materials Science and Engineering: C. 2021;118:111353.
8. Nguyen CV, Dao TP, Tho TT, Hoa LT, Hieu NN, Phuc HV, et al. Understanding the electronic properties, contact types and optical performances in graphene/InN heterostructure: Role of electric gating. Diamond and Related Materials. 2020;106:107851.
9. Su F, Wu Z-S. A perspective on graphene for supercapacitors: Current status and future challenges. Journal of Energy Chemistry. 2021;53:354-7.
10. Das A, Mondal SR, Palai G. Realization of graphene based quantum dot solar cell through the principle of photonics. Optik. 2020;221:165283.
11. Siahlo AI, Popov AM, Poklonski NA, Lozovik YE, Vyrko SA, Ratkevich SV. Multi-layer graphene membrane based memory cell. Physica E: Low-dimensional Systems and Nanostructures. 2016;84:348-53.
12. Gaj J, Clapa M, Nowak D, Juszczak J, Galazka M, Pelka M, et al. Metallurgical graphene under different gas atmospheres and UV radiation for gas-sensing applications. Sensors and Actuators A: Physical. 2020;312:112152.
13. Tang Y, Tian J, Li S, Xue C, Xue Z, Yin D, et al. Combined effects of graphene oxide and Cd on the photosynthetic capacity and survival of Microcystis aeruginosa. Science of The Total Environment. 2015;532:154-61.
14. Zhao W-H, Yang L-J, Qing L-H, Lv X-M, Yi L-Y, Li H, et al. The strong effect of substituents on the carbonyl reduction in graphene oxide: A DFT study. Computational and Theoretical Chemistry. 2015;1068:1-7.
15. Yu L, Shi M, Yue X, Qu L. A novel and sensitive hexadecyltrimethyl ammonium bromide functionalized graphene supported platinum nanoparticles composite modified glassy carbon electrode for determination of sunset yellow in soft drinks. Sensors and Actuators B: Chemical. 2015;209:1-8.
16. Das Sarma S, Adam S, Hwang EH, Rossi E. Electronic transport in two-dimensional graphene. Reviews of Modern Physics. 2011;83(2):407-70.
17. Wang Y, Tong SW, Xu XF, Özyilmaz B, Loh KP. Interface Engineering of Layer-by-Layer Stacked Graphene Anodes for High-Performance Organic Solar Cells. Advanced Materials. 2011;23(13):1514-8.
18. Balandin AA. Thermal properties of graphene and nanostructured carbon materials. Nature Materials. 2011;10(8):569-81.
19. Kim T, Jung G, Yoo S, Suh KS, Ruoff RS. Activated Graphene-Based Carbons as Supercapacitor Electrodes with Macro- and Mesopores. ACS Nano. 2013;7(8):6899-905.
20. Yang H, Hernandez Y, Schlierf A, Felten A, Eckmann A, Johal S, et al. A simple method for graphene production based

on exfoliation of graphite in water using 1-pyrenesulfonic acid sodium salt. Carbon. 2013;53:357-65.
21. Liu Y, Tourbin M, Lachaize S, Guiraud P. Silica nanoparticles separation from water: Aggregation by cetyltrimethylammonium bromide (CTAB). Chemosphere. 2013;92(6):681-7.
22. Vaghri E, Dorranian D, Ghoranneviss M. Effects of CTAB concentration on the quality of graphene oxide nanosheets produced by green laser ablation. Materials Chemistry and Physics. 2018;203:235-42.
23. Díez-Pascual AM, Vallés C, Mateos R, Vera-López S, Kinloch IA, Andrés MPS. Influence of surfactants of different nature and chain length on the morphology, thermal stability and sheet resistance of graphene. Soft Matter. 2018;14(29):6013-23.
24. Zamiranvari A, Solati E, Dorranian D. Effect of CTAB concentration on the properties of graphene nanosheet produced by laser ablation. Optics & Laser Technology. 2017;97:209-18.
25. Du H, Castaing V, Guo D, Viana B. Rare-earths doped-nanoparticles prepared by pulsed laser ablation in liquids. Ceramics International. 2020;46(16):26299-308.
26. Mortazavi SZ, Parvin P, Reyhani A. Fabrication of graphene based on Q-switched Nd:YAG laser ablation of graphite target in liquid nitrogen. Laser Physics Letters. 2012;9(7):547-52.
27. Ghavidel E, Sari AH, Dorranian D. Experimental investigation of the effects of different liquid environments on the graphene oxide produced by laser ablation method. Optics & Laser Technology. 2018;103:155-62.
28. Mahdian Asl P, Dorranian D. Effect of liquid medium temperature on the production rate and quality of graphene nanosheets produced by laser ablation. Optical and Quantum Electronics. 2016;48(12).
29. Solati E, Vaghri E, Dorranian D. Effects of wavelength and fluence on the graphene nanosheets produced by pulsed laser ablation. Applied Physics A. 2018;124(11).
30. Vaghri E, Dorranian D. Effects of green laser fluence on the characteristics of graphene nanosheets synthesized by laser ablation method in liquid nitrogen medium. Optical and Quantum Electronics. 2018;50(2).
31. Abramov D, Arakelian S, Kochuev D, Makov S, Prokoshev V, Khorkov K. Interaction of femtosecond laser radiation with carbon materials: exfoliation of graphene structures and synthesis of low-dimensional carbon structures. Nanosystems: Physics, Chemistry, Mathematics. 2016:220-5.
32. Khatamian M, Khodakarampoor N, Saket Oskoui M, Kazemian N. Synthesis and characterization of RGO/zeolite composites for the removal of arsenic from contaminated water. RSC Advances. 2015;5(45):35352-60.
33. Miao J, Liu H, Li W, Zhang X. Mussel-Inspired Polydopamine-Functionalized Graphene as a Conductive Adhesion Promoter and Protective Layer for Silver Nanowire Transparent Electrodes. Langmuir. 2016;32(21):5365-72.
34. Wong C, Lai C, Lee K, Hamid S. Advanced Chemical Reduction of Reduced Graphene Oxide and Its Photocatalytic Activity in Degrading Reactive Black 5. Materials. 2015;8(10):7118-28.
35. Vaghri E, Khalaj Z, Dorranian D. Investigating the Effects of Different Liquid Environments on the Characteristics of Multilayer Graphene and Graphene Oxide Nanosheets Synthesized by Green Laser Ablation Method. Diamond and Related Materials. 2020;103:107697.
36. Mansor N, Jorge AB, Corà F, Gibbs C, Jervis R, McMillan PF, et al. Graphitic Carbon Nitride Supported Catalysts for Polymer Electrolyte Fuel Cells. The Journal of Physical Chemistry C. 2014;118(13):6831-8.
37. Tuinstra F, Koenig JL. Raman Spectrum of Graphite. The Journal of Chemical Physics. 1970;53(3):1126-30.
38. Maultzsch J, Reich S, Thomsen C. Double-resonant Raman scattering in graphite: Interference effects, selection rules, and phonon dispersion. Physical Review B. 2004;70(15).
39. Frank O, Mohr M, Maultzsch J, Thomsen C, Riaz I, Jalil R, et al. Raman 2D-Band Splitting in Graphene: Theory and Experiment. ACS Nano. 2011;5(3):2231-9.
40. Kaniyoor A, Ramaprabhu S. A Raman spectroscopic investigation of graphite oxide derived graphene. AIP Advances. 2012;2(3):032183.
41. Cheng YH, Tay BK, Lau SP, Shi X, Qiao XL, Chen JG, et al. Raman spectroscopy of carbon nitride films deposited using the filtered cathodic vacuum-arc technique combined with a radio-frequency nitrogen-ion beam. Applied Physics A Materials Science & Processing. 2001;73(3):341-5.
42. Popov M, Churkin V, Kirichenko A, Denisov V, Ovsyannikov D, Kulnitskiy B, et al. Raman Spectra and Bulk Modulus of Nanodiamond in a Size Interval of 2–5 nm. Nanoscale Research Letters. 2017;12(1).
43. Zhu Y, Laipan M, Zhu R, Xu T, Liu J, Zhu J, et al. Enhanced photocatalytic activity of Zn/Ti-LDH via hybridizing with C60. Molecular Catalysis. 2017;427:54-61.
44. Motahari H, Malekfar R. Laser Micro-Raman Spectroscopy of CVD Nanocrystalline Diamond Thin Film. International Journal of Optics and Photonics. 2019;13(1):3-12.
45. Díez-Pascual AM, Vallés C, Mateos R, Vera-López S, Kinloch IA, Andrés MPS. Influence of surfactants of different nature and chain length on the morphology, thermal stability and sheet resistance of graphene. Soft Matter. 2018;14(29):6013-23.
46. Wang H, Zeuschner J, Eremets M, Troyan I, Willams J. Stable solid and aqueous H2CO3 from CO2 and H2O at high pressure and high temperature. Scientific Reports. 2016;6(1).
47. Dar MA, Kim Y-S, Ansari SG, Kim H-i, Khang G, Van Chiem C, et al. Comparative study of diamond films grown on silicon substrate using microwave plasma chemical vapor deposition and hot-filament chemical vapor deposition technique. Korean Journal of Chemical Engineering. 2005;22(5):770-3.
48. Chu PK, Li L. Characterization of amorphous and nanocrystalline carbon films. Materials Chemistry and Physics. 2006;96(2-3):253-77.
49. Cheng M, Yang R, Zhang L, Shi Z, Yang W, Wang D, et al. Restoration of graphene from graphene oxide by defect repair. Carbon. 2012;50(7):2581-7.
50. Krishnamoorthy K, Veerapandian M, Yun K, Kim SJ. The chemical and structural analysis of graphene oxide with different degrees of oxidation. Carbon. 2013;53:38-49.
51. Muzyka R, Drewniak S, Pustelny T, Chrubasik M, Gryglewicz G. Characterization of Graphite Oxide and Reduced Graphene Oxide Obtained from Different Graphite Precursors and Oxidized by Different Methods Using Raman Spectroscopy. Materials. 2018;11(7):1050.
52. Cervantes-Cuevas H, Jiménez-Hernández M, Chavez-Esquivel G, Acosta D, Tavizon-Pozos JA, Santolalla-Vargas CE, et al. Effect of different coupling agents in the doping of graphite oxide with 3–3′ diaminobenzidine: textural, structural and electrical properties. Materials Research Express.

2020;7(2):025603.
53. Singh G, Choudhary A, Haranath D, Joshi AG, Singh N, Singh S, et al. ZnO decorated luminescent graphene as a potential gas sensor at room temperature. Carbon. 2012;50(2):385-94.
54. Kannan S. FT-IR and EDS analysis of the seaweeds Sargassum wightii (brown algae) and Gracilaria corticata (red algae), Int.J.Curr.Microbiol.App.Sci. 2014;3(4):341-351.
55. Fan Y, Liu Y, Cai Q, Liu Y, Zhang J. Synthesis of CTAB-intercalated graphene/polypyrrole nanocomposites via in situ oxidative polymerization. Synthetic Metals. 2012;162(21-22):1815-21.
56. Yazid SNAM, Isa IM, Bakar SA, Hashim N. Facile, cost effective and green synthesis of graphene in alkaline aqueous solution. Int. J. Electrochem. Sci. 2015; 10(10):7977-7984.
57. Özdemir Öge T. FT-IR, Laser-Raman, UV-Vis, and NMR Spectroscopic Studies of Antidiabetic Molecule Nateglinide. Journal of Spectroscopy. 2018;2018:1-12.